

Article @ Virology

Immunogold Nanoparticles Recognition imaging by Direct Atomic Force Microscopy

Yang Cao¹ †, Wenwen Zhang² †, Pengfei Yang³ †, Liping Zhang¹ †, Lili Li¹, Xin Zhao¹, Jinke Li¹, Xuezheng Ma¹, Ruijin Ping¹, and Kongxin Hu¹ *

1. Chinese Academy of Inspection and Quarantine, Beijing 100123, China;

2 Beijing International Travel Healthcare center, Beijing 100026, China;

3 Huaian Center for Disease Control and Prevention, 223300, Huaian, Jiangsu province, China

ABSTRACT

We have developed a method that integrated the widely used nanogold immunoassay into direct atomic force microscopy (AFM) imaging and provided a specific morphological technique applying for virus identification. The series of specimens including bare gold particles (Au), antibody-conjugated gold particles (Au-Ab), purified influenza virions (H1N1), antibody-bound virions (H1N1-Ab) and virion-immunogold complex (H1N1-Ab-Au) were investigated by AFM and transmission electron microscopy stepwisely and parallelly. The recognition method of the immuno-AFM technique was constructed by taking the local phase contrast in phase image as main judgment for the existence of immunogold labels and taking the height and amplitude images as auxiliary judgment for viral morphology and positioning. The nanogold-antibody conjugates binding to the H1N1 virions were clearly identified as higher brightness spots from the background biomaterials. Under direct AFM, the topographical image of the scanned biosamples can be easily investigated and reproduced. Our findings achieved the combination of virus morphological features with antibody-antigen specific recognition through the application of antibody-specific nanogold labels and, in principle, the labels for immuno-AFM could be extended to other types of nanomaterials for bio-recognition and localization assay.

Copyright©2012-2020 Published by Hong Kong Institute of Biologicals Standardization Limited. All rights reserved.

Article history: Submitted: 01/11/2017; Revised: 28/11/2017; Accepted: 30/11/2017

DOI: 10.21092/jav.v6i4.95

Key Words: Direct Atomic Force Microscopy; Immunogold; Nanoparticles; influenza virions

* Corresponding author, Prof. Kongxin Hu, PhD. , Major in Immunology

Tel: +86-10-53897796 E-mail: hukongxin@caiq.gov.cn

†These authors contributed equally to this work.

Copyright©2012-2020 Published by Hongkong Institute of Biologicals Standardization Limited.

All rights reserved.

Material and method

1. Materials

1.1 Antibody labeling of immunogold nanoparticles

Colloidal gold nanoparticles were prepared by Natan method^[1]. Briefly, 100 ml deionized water was heated to boil. 1ml of 1% HAuCl₄ solution was added slowly following by addition of 4ml of 1% sodium citrate with continuous heating and vigorously stirring until the tetrachloroauric solution turned claret. Average diameter of colloidal gold particles was estimated to be approximate 15-20nm as detected by transmission electron microscopy.

Monoclonal antibody to H1N1 virus Type A Hemagglutinin H1 (mouse anti-HA MAb, clone B214M, Meridian Life Science) was immobilized on the surface of colloidal gold particles as following. Colloidal gold solution with A₂₅₀=1.0 was titrated with 0.2M K₂CO₃ to pH8.5, and antibody solution (0.1mg/ml) in 10mM Tris-HCl, pH8.5, was added. BSA (Sigma-Aldrich) was added to a final concentration of 0.1% for additional stabilization of the resulting MAb complex with gold nanoparticles. To remove non-bounded antibodies, the mixture was centrifuged for 45 min at 10,000rpm and 4°C. The pellet was resuspended in 0.05M K-phosphate buffers (pH7.5, 0.01% NaN₃, 0.1% BSA). The resulting immunogold particles (MAb-Au) were stored at 4°C. Mouse IgG2a isotype control antibody (clone 20102, R&D) was used as control in

some experiments.

1.2 H1N1 virus sample

H1N1 influenza virus (Influenza A/New Caledonia/20/99) was a gift from Dr. Qi Fengchun (Department of Influenza vaccine, Changchun Institute of Biological Products, China). The virus was purified by ultracentrifugation with 10-40% sucrose gradient.

1.3 Preparation of gold nanoparticle and virus samples for AFM imaging

Bare Au nanoparticle, Au-Ab nanoparticle or H1N1 virus samples were diluted with 0.01mM PBS. 50µl of each sample was uniformly coated on poly-L-lysine(Sigma-Aldrich) pretreated coverslip and incubated at 37 °C for 30min, following by washing with deionized water for three times and blow-drying by nitrogen for imaging.

If preparing H1N1-Ab sample or Au-Ab particles for AFM imaging, further treatment were necessary as following: coverslip was incubated for 30min covered by 10% BSA. After washing with deionized water, 50µl of immunogold particles (or 50 µl 3.5µg/ml MAb containing 0.01% Tween 20) were placed on coverslip carrying samples and the coverslip was incubated at 37°C for 30min, following by washing and blow-drying by nitrogen for AFM imaging. Special attention should be addressed to Au nanoparticles, with which operation should be performed gently.

1.4 Atomic force microscopy imaging

AFM images were collected using Multimode equipment and NanoScope IIIa controller (Digital Instruments Co., Santa Barbara). Tapping mode and 115 μ m-length standard silicon cantilevers were employed for imaging in air. RTESP tips (Veeco Instruments) with spring constant 20-80N/m and tip radius 5-10nm were used with a resonant frequency of approximate 300 kHz, and a scanning speed of 1-5 Hz. We generally adjusted the set point of voltage for optimum image quality. The height, amplitude and phase data were recorded simultaneously at a scan rate of 2 Hz, and

the 256 \times 256 pixel and 512 \times 512 pixel images were collected at a scan-rate of one scan lines per second. All images and data were evaluated by Nanoscope Software (Nanoscope version 6.13R1, Digital Instruments) or XEI Image Processing Software (XEI version 1.6, PSIA Corp.). Other AFM experimental procedures and parameters were performed as described previously^[2-4].

1.5 Transmission electron microscopy

A double-staining immunoelectron microscopy was used in this study. 6 μ l of resuspended samples were applied to carbon coated copper grid and left to stand for 1-2 min at room temperature. Excess liquid was gently removed away using Whatman paper and 6 μ l of negative stain (2% potassium phosphotungstate, pH 6.8) was added to the grids. Excess stain was removed and the

grids were dried at room temperature. Samples were examined at an acceleration voltage of 80 kV with a TECNAI12 transmission electron microscopy (FEI).

Results & Discussion

It is well known that detection of virus by immunoelectron microscopy (IEM) is more sensitive than by direct transmission electron microscopy (TEM) alone. With the application of electron dense of gold nanoparticles, IEM technology can achieve combination of specific biolabel location with nanoscale imaging techniques, and is kept as a “gold standard” for identification of non-cultivable viruses^[5-6]. As a companion technique to TEM, AFM^[7] is a unique technique to provide subnanometer resolution under physiological conditions^[8]. Over the past years, with great efforts on sample preparation, imaging techniques and instrumentation, AFM complemented TEM by allowing visualization of biological samples, such as proteins, nucleotides, viruses, membranes, and living cells^[2,9-12]. Theoretically, introduction of immunolabeling technique into AFM would achieve direct visualization of the immunolabels' locations within bio-specimen at nanoscale, which could be potentially developed as a substitute for IEM.

However, unlike IEM, AFM uses a tiny, pointed probe instead of lens. When the

tip of the probe rides gently on the sample, its up-and-down motion is recorded and displayed as images on computer. Since the imaging principle of the AFM is significantly different from IEM, AFM imaging could not highlight the nanogold biolabels as electron dense dots. Previous studies on bio-recognition, inter- and intra-molecular interactions have been reported, as exemplified by analysis of ligand-receptor adhesion^[13], antibody-antigen interaction^[14,15], enzyme recognition processes^[16], polysaccharide elasticity^[17,18], DNA mechanics^[19,20] and function of molecular motors^[21,22]. However, the usage of modified probes with ligands may result in the morphological features of the scanned bio-specimen hard to be reproduced and calibrated. Consequently, the specific bio-recognition process could not combine with the “ true ” morphology of bio-specimen.

Here we developed a specific nanoscale morphological technique that integrated immunogold labeling assay into direct AFM imaging. Since the sample homogeneity appeared to be essential for good AFM imaging^[23], we used purified H1N1 viruses as the target biosample. Specimens, including bare Au particles, Au-Ab particles, purified H1N1 virions, H1N1-Ab, H1N1-Ab-Au, were investigated by both AFM and TEM with purposes of well-displaying and comparing the possible label signals of immunogold nanoparticles.

All AFM imagings were performed in constant tapping force in air and output data types were set as height, amplitude and phase simultaneously.

Initially, we investigated bare Au nanoparticles. No significant differences were found in the pattern of gold nanoparticles between AFM height, amplitude, phase images (Fig. 1a, b,c) and TEM control (Fig. 1d). All bare gold particles were regular and circular shapes with a diameter approximately 15-20nm. Comprehensive analysis of the height, amplitude and phase data showed that the morphologic contour, particles distribution and size of the gold particles displayed high consistency in all three imaging modes.

We next investigated topographic features of Au particles coated with H1N1 MAb (Au-Ab). Interestingly, the morphologic contour of the particles observed in phase image (Fig. 1g) showed apparent inconsistency compared with the corresponding appearance of particles observed in height and amplitude images (Fig. 1e, f). Disappeared regions and irregular contour of Au-Ab particles were found more often in phase image and the Au-Ab particles were emerged in higher brightness form (intense phase contrast) while some other parts were merged into background (Fig. 1g). Further section analysis of aggregated Au-Ab particles displayed significant divergences in

particle morphology in height, amplitude and phase images as shown in black circle area in Fig. 1e, f, g. Those intact aggregated Au-Ab particles shown in height and amplitude modes kept adjacent performance (Fig. 1i, j), while, the particles appeared as separated and non-intact distribution with intense brightness features in phase (Fig. 1k). The phenomenon indicated that some areas of the immunogolds were covered with or buried under the background phase signals and the irregular “intense brightness areas” in phase image must be signals for existence of Au nanoparticles in the protein-mixed materials. As a control, TEM image of the Au-Ab nanoparticles still displayed as intact spherical particles in bold dark dots form with a little fuzzy around (Fig. 1h). Taken together, the irregular higher brightness areas in AFM phase image gave us a clue that the immunogold could be developed as biolabel on direct AFM.

Purified H1N1 viruses were then imaged through AFM and TEM. The AFM height (Fig. 2a), amplitude (Fig. 2b) and phase (Fig. 2c) images displayed high consistency in virion distribution and also morphological features. TEM image of the purified H1N1 virions displayed intact spherical particles with characteristic “spikes” (Fig. 2d). AFM and TEM imaging of H1N1-Ab complexes were also investigated. The height, amplitude and phase data of the H1N1-Ab were highly identical regarding to shapes and distribution of both spherical and

filamentous H1N1 virions. Compared to height and amplitude images (Fig. 2e, f), phase image (Fig. 2g) displayed more detailed background components and lots of smaller particles (presumably immunoglobulin molecules) could be observed on or beside spherical/filamentous H1N1 particles. TEM images (Fig. 2h) of H1N1-Ab still displayed intact morphological features except a little faintness appeared on virus particles when compared with TEM image of the pure viruses without bound antibodies (refer to Fig. 2d).

Finally, H1N1-Ab-Au complex images from different scan fields on the sample glass coverslip were scanned by AFM at scan size as $600\text{nm} \times 600\text{nm}$, $300\text{nm} \times 300\text{nm}$ and $200\text{nm} \times 200\text{nm}$ individually. The topographical features of H1N1 particles were still clear and visible on height and amplitude images. Many “higher brightness spots” were observed apparently in the phase image (Fig. 3c,g,k) and these spots could not be found in the corresponding height (Fig. 3a,e,i) and amplitude images (Fig. 3b,f,j). Moreover, we found these contrast signals in phase appeared as “pits” on or beside virions surface in the corresponding amplitude image (Fig. 3b,f,j). As a control, TEM image of H1N1-Ab-Au complex sample was performed, and some “intense black dots”, known as high electron dense immunogold particles, were visualized on or beside H1N1 virions (Fig. 3d, h).

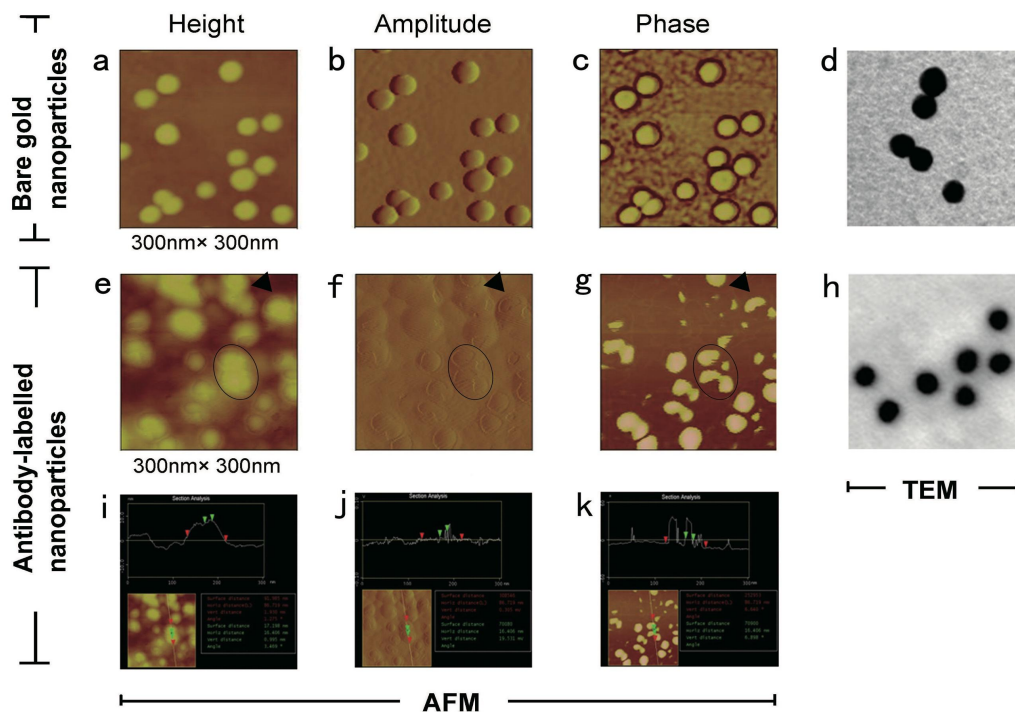


Figure1 : AFM and TEM images of bare nanogold particles and nanogold particles labeled with MAb to influenza A H1.

(a-c) AFM images of freshly prepared bare Au nanoparticles (about 15-20 nm diameter) spread on poly-L-Lysine pretreated coverslips. Imaging (Scan size: 300nm× 300nm) of particles was scanned in tapping mode and displayed as height image (a), amplitude image (b), and phase image (c). (d) TEM image of freshly prepared Au nanoparticles. Au particles were shown as electron dense dots. (e-h) Images of Au-Ab (immunogold particles) scanned by AFM and TEM. AFM imaging (Scan size: 300nm× 300nm) of immunogold particles was performed and displayed as height (e), amplitude (f) and phase (g) images. Black arrows indicated image of a same virus particle in different data type of AFM, revealing absolutely different particle shapes among the three data types. (h) TEM image of prepared immunogold particles. Electron dense dots represented immunogold particles targeted against Hemagglutinin H1 protein of H1N1 virus, displaying intact spherical shape of gold particles. (i-k) Images of section analysis of aggregated immunogold particles, indicated by black circles in the corresponding AFM images in Fig. 1e, f and g. Height (i), amplitude (j) and phase (k) images displayed significant divergence in particle morphology.

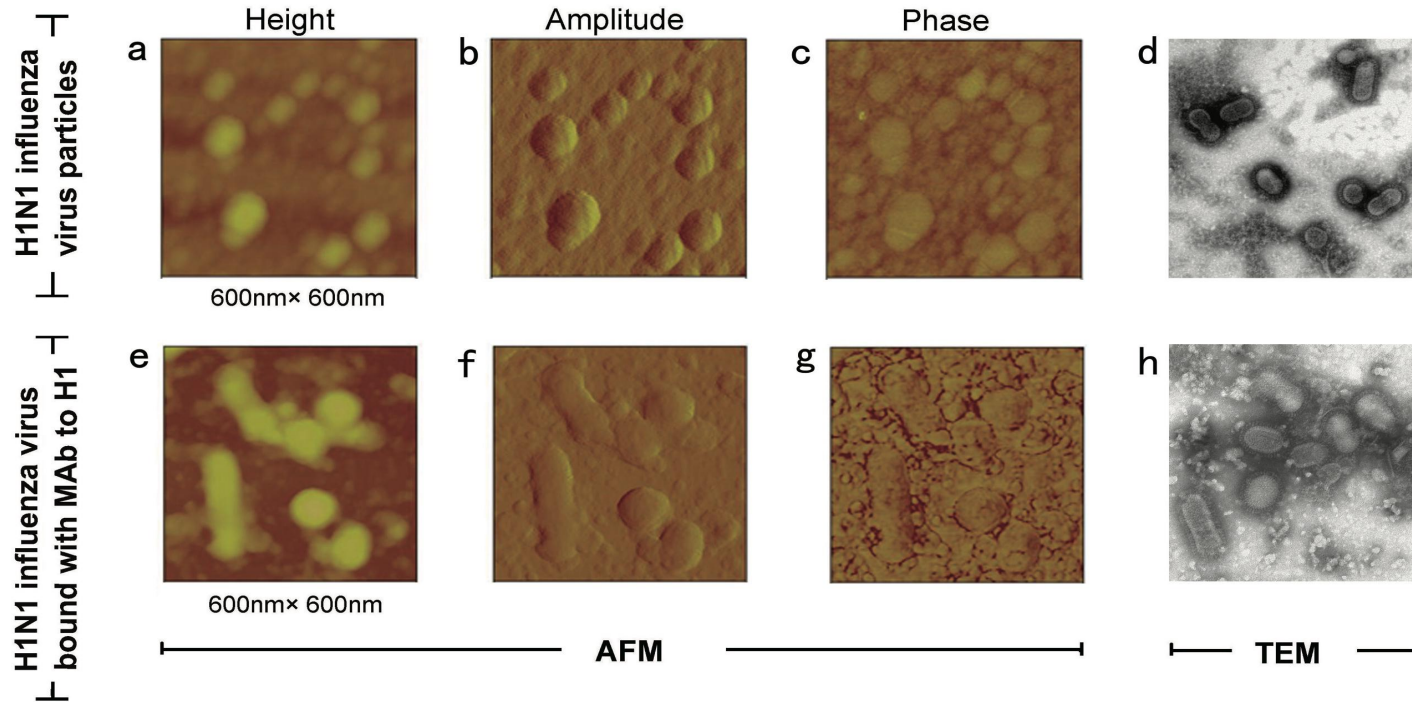


Figure 2: AFM and TEM images of H1N1 virus (a-d) and H1N1-Ab (virus bound with MAb to Hemagglutinin H1) (e-h).

(a-c) AFM images of purified H1N1 virus. Imaging of H1N1 virus particles was scanned in tapping mode and displayed as height (a), amplitude (b) and phase (c) images. (d) TEM image of purified H1N1 influenza virus particles, displaying intact morphological features of influenza virus. (e-g) AFM imaging of H1N1-Ab complexes was performed in tapping mode and displayed as height (e), amplitude (f) and phase (g) images. (h) TEM image of H1N1-Ab complex, displaying classic morphological features of influenza virus, except a little faintness appeared on virus particles compared with TEM image of the purified viruses.

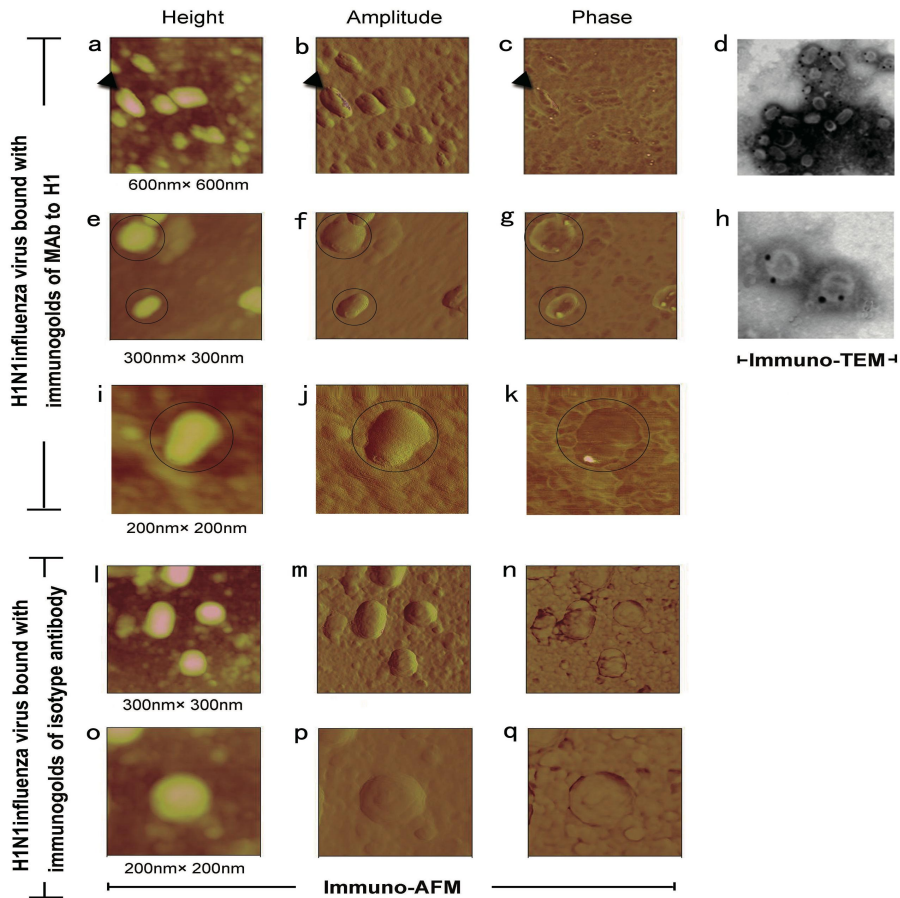


Figure 3: AFM and TEM images of H1N1-Ab-Au (H1N1 virion-immunogold complex)

(a-c) AFM images of H1N1-Ab-Au. Imaging (scan size: 600nm×600nm) was scanned in tapping mode and displayed as height (a), amplitude (b) and phase (c) images at 600×600 nm size. (d) TEM image of H1N1-Ab-Au, displaying as “electron dense dots” binding to H1N1 virus particles. (e-g) H1N1-Ab-Au complexes were scanned by AFM at scan size 300nm×300nm and the output data were displayed as height (e), amplitude (f) and phase (g) images. (h) TEM image of H1N1-Ab-Au complexes at increasing magnification. (i-k) single immunogold binding H1N1 virus particle (scan size: 200nm×200nm) was displayed as height (i), amplitude (j) and phase (k) images. Three arrows/circles in a horizontal row indicated image of a same virus particle, revealing similar particle shapes in height, amplitude and phase data type. (l-q) Control AFM images of H1N1 virions bound with immunogolds of IgG 2a isotype antibody. Images were scanned at 300nm× 300nm size for height (l), amplitude (m) and phase (n) images, or at 200nm×200nm size for height (o), amplitude (p) and phase images (q).

The origin of the phase contrast is from the difference in probe-sample interaction, which heavily depends on the viscoelasticity of the material under scrutiny. Previous study showed phase images recorded at moderate tapping were related to surface stiffness variations associated with Young's modulus change^[1]. Au particles are much harder than the biomaterial samples as virion, immunoglobulin and bovine serum albumin (BSA) employed here, and produce stronger interaction when probe taps on them. This is why the Au particles appeared as bright spots in phase image (Fig. 3c,g,k). Meanwhile, higher interaction force causes decrease of amplitude, shown as pits in amplitude image (Fig 3b,f,j).

The boundary between two objects shows difference in effective viscoelasticity even they are same in material. For example, the boundary or the gap between H1N1 virion and the bound immunogold particle may have different interaction from both parts, which produces contrast in phase, as shown in Fig. 3k. However, the gap might be much smaller than the probe size and probe could not insert into it. Therefore, the gap between two parts cannot be observed in height and amplitude images, as shown in Fig. 3i and Fig. 3j.

Our data also showed that intense phase contrast might lead a little decreasing of quality of viral particle imaging when goldparticles appeared on phase image (Fig. 3c, g, k). Interestingly, the simultaneous

outputting height and amplitude images seemed no loss of quality (Fig. 3c, g, k). Therefore, comprehensive analysis of both the local “higher bright spots” on phase image and the distributional features of viral morphology on height and amplitude images would be critical for specific virus identification by immuno-AFM. In contrast, no “higher brightness spots” signals were found binding to H1N1 virions when nonspecific isotype antibody was used as negative control to prepare Au-Ab particles (Fig. 3l, m, n, o, p, q), which indicated low to undetectable nonspecific signals were detected.

Additionally, we also found that a minority of Au-Ab particle was difficult to display on phase image (Fig. 1g), which implicated that sensitivity of this specific morphological immunoassay would be lost a little since a small proportion of Au-Ab labels lost signals inevitably. Thus, the Au particle may be probably not the best label candidate for application of immuno-AFM. However, it should be also noted that the “classic” IEM labeling marker-goldparticle was chosen in present study, because it provided a best reference at nanometer-scale to evaluate methodology of immuno-AFM. Based on the principle of this study, some improvements within labeling materials should be expected in the future.

Conclusion

By comprehensive analysis of the “higher bright spots” as immunogold label signals in phase image and the distributional characteristics of viral topography appeared on height and amplitude images, we have demonstrated an immuno-AFM technique to detect H1N1 virus, which achieved specific differentiation of signals of the nanogold bio-labels from the background biomaterials. Our studies integrated the micro-high-resolution imaging performance of AFM with the specificity of antibody recognition and opened up a methodology for screening AFM bio-labels. As specific bio-recognition and morphological images can be obtained at the same time during this process and the labeling methodology is applicable with any ligand, it should prove possible to recognize and position many types of biomaterials on a nanometer scale.

Acknowledgements

We are grateful to Drs. Wanxin Sun and Dengli Qiu for enlightening discussions. This work was supported by the National key research and development plan (2016YFC1200904 and 2017YFC1201100), The state key development program (2016 YFF0103103)

References

- [1]. Freeman R G, Grabar K C, Allison K J, et al. Self-assembled metal colloid monolayers: an approach to SERS substrates [J]. *Science*, 1995, 267(5204): 1629-1632.
- [2]. Kuznetsov Y G, Malkin A J, Lucas R W, et al. Imaging of viruses by atomic force microscopy[J]. *Journal of General Virology*, 2001, 82(9): 2025-2034.
- [3]. Malkin A J, Kuznetsov Y G, Lucas R W, et al. Surface processes in the crystallization of turnip yellow mosaic virus visualized by atomic force microscopy[J]. *Journal of structural biology*, 1999, 127(1): 35-43.
- [4]. Plomp M, Rice M K, Wagner E K, et al. Rapid visualization at high resolution of pathogens by atomic force microscopy: structural studies of herpes simplex virus-1[J]. *The American journal of pathology*, 2002, 160(6): 1959-1966.
- [5]. Doane F W. Immunoelectron microscopy in diagnostic virology[J]. *Ultrastructural pathology*, 1987, 11(5-6): 681-685.
- [6]. Singer S J. Preparation of an electron-dense antibody conjugate[J]. *Nature*, 1959, 183(4674): 1523-1524.
- [7]. Binnig G, Quate C F, Gerber C. Atomic force microscope[J]. *Physical review letters*, 1986, 56(9): 930.
- [8]. Kada G, Kienberger F, Hinterdorfer P. Atomic force microscopy in bionanotechnology[J]. *Nano Today*, 2008, 3(1): 12-19.

- [9]. Engel A, Müller D J. Observing single biomolecules at work with the atomic force microscope[J]. *Nature Structural & Molecular Biology*, 2000, 7(9): 715-718.
- [10]. Horber J K H, Miles M J. Scanning probe evolution in biology[J]. *Science*, 2003, 302(5647): 1002.
- [11]. Allison D P, Hinterdorfer P, Han W. Biomolecular force measurements and the atomic force microscope[J]. *Current Opinion in Biotechnology*, 2002, 13(1): 47-51.
- [12]. Bhushan B, Fuchs H. Applied scanning probe methods VII[M]. Springer-Verlag Berlin Heidelberg, 2006,143-165.
- [13]. Florin E L, Moy V T, Gaub H E. Adhesion forces between individual ligand-receptor pairs[J]. *Science-AAAS-Weekly Paper Edition-including Guide to Scientific Information*, 1994, 264(5157): 415-417.
- [14]. Raab A, Han W, Badt D, et al. Antibody recognition imaging by force microscopy[J]. *Nature biotechnology*, 1999, 17(9): 901-905.
- [15]. Ouerghi O, Touhami A, Othmane A, et al. Investigating specific antigen/antibody binding with the atomic force microscope[J]. *Biomolecular engineering*, 2002, 19(2): 183-188.
- [16]. Radmacher M, Fritz M, Hansma H G, et al. Direct observation of enzyme activity with the atomic force microscope[J]. *Science*, 1994: 1577-1577.
- [17]. Rief M, Oesterhelt F, Heymann B, et al. Single molecule force spectroscopy on polysaccharides by atomic force microscopy[J]. *Science*, 1997, 275(5304): 1295-1297.
- [18]. Marszalek P E, Oberhauser A F, Pang Y P, et al. Polysaccharide elasticity governed by chair-boat transitions of the glucopyranose ring[J]. *Nature*, 1998, 396(6712): 661-664.
- [19]. Smith S B, Cui Y, Bustamante C. Overstretching B-DNA: the elastic response of individual double-stranded and single-stranded DNA molecules[J]. *Science*, 1996: 795-799.
- [20]. Strick T R, Allemand J F, Bensimon D, et al. The elasticity of a single supercoiled DNA molecule[J]. *Science*, 1996, 271(5257): 1835-1837.
- [21]. Veigel C, Coluccio L M, Jontes J D, et al. The motor protein myosin-I produces its working stroke in two steps[J]. *Nature*, 1999, 398(6727): 530-533.
- [22]. Tanaka H, Homma K, Iwane A H, et al. The motor domain determines the large step of myosin-V[J]. *Nature*, 2002, 415(6868): 192-195.
- [23]. Lee J W M, Ng M L. A nano-view of West Nile virus-induced cellular changes during infection[J]. *Journal of Nanobiotechnology*, 2004, 2(1): 6.